FACHHOCHSCHULE **TRIER**
Hochschule für Technik, Wirtschaft und Gestaltung
University of Applied Sciences
Informatik

Informatik-Bericht Nr. 2012-3

Schriftenreihe Fachbereich Informatik, Fachhochschule Trier

Published: BMT 2012 – 46. DGBMT Jahrestagung, Jena (for internal use)

Improvements on the Feasibility of Active Shape Model-based Subthalamic Nucleus Segmentation

F. Bernard[1], P. Gemmar[1], A. Husch[1], F. Hertel[2]

[1]Institute for Innovative Informatics Applications i3A,
Trier University of Applied Sciences, Trier, Germany
[2]Centre Hospitalier de Luxembourg, Luxembourg (City), Luxembourg

Abstract

Finding the location and morphology of subcortical structures in the human brain is of crucial importance for deep-brain-stimulation (DBS). DBS of the subthalamic nucleus (STN) is used as a treatment for Parkinson's disease (PD) requiring accurate target positioning. However, segmenting the STN automatically is difficult because it is not clearly visible in magnetic resonance imaging (MRI). In this publication an improvement on the feasibility of an approach based on active shape models (ASM) for the automatic localisation of the STN is presented.

1 Introduction

1.1 Background

Deep-brain-stimulation (DBS) is a common treatment for diseases such as dystonia or advanced Parkinson's disease (PD). DBS uses electrodes implanted into a particular brain region in order to stimulate or inhibit neural activity.

In order to navigate the electrode accurately to the optimal position it is of crucial importance for the physician to know the exact location of the electrode's target area prior to the surgery. For PD treatment the electrodes are usually implanted in the area of the subthalamic nucleus (STN). A major problem of directly locating the STN is that it is not clearly visible in magnetic resonance imaging (MRI). Therefore the STN is commonly located using an indirect approach based on STN coordinates taken from an atlas or other literature [1]. However, using such a general procedure is inaccurate due to the wide variability of the STN shape and position amongst patients. Due to these reasons an individual STN localisation based on each patient's MRI record is desirable.
Our long-term aim is to develop a system that is able to assist physicians before and during DBS surgeries in order to increase the safety of the intervention and to reduce stress for both patient and surgeon. For the planning and navigation module of this system a (semi)-automatic STN segmentation is required. In this publication the first part towards the automatic STN segmentation is presented.
However, as the STN and the adjacent substantia nigra (SNr) are not visually discriminable in MRI, both structures are segmented together (referred to as SNr-STN) in our approach. The STN is then extracted from the SNr-STN using a statistical approach.

1.2 Point Distribution Models

To address the segmentation of the SNr-STN, a method based on active shape models (ASM) [2] has been chosen.

1.2.1 Active Shape Models

ASM require a set of N 3D training images $(I_1,...,I_N)$, each image I_j being annotated with a set X_j of consistent landmarks that correspond to the same location of the SNr-STN in all images $I_1,...,I_N$. For each image I_j the landmarks X_j consist of a column vector with length 3M, with M being the number of landmarks (constant) and the elements of X_j with index 1,...,M, (M+1),...,(2M) and (2M+1),...,(3M) representing the x, y and z coordinates of each landmark. These landmarks form a discrete grid in 3D space that represents an approximation of the SNr-STN's shape. For data dimension reduction and modelling the shape variability of the SNr-STN (represented by the landmarks), the principal components of the covariance matrix of the landmarks are determined using principal component analysis (PCA). Let $v_1,...,v_k$ be the eigenvectors of the covariance matrix of the landmarks that correspond to the k largest eigenvalues that were determined by the PCA. The number of eigenvectors k is chosen so that a given proportion of the training data's variance is expressed. With X_{mean} being the mean of $X_1,...,X_N$, the shape X' can be reconstructed, with respect to the proportion of variance, using the approximation $X' \approx X_{mean} + [v_1,...,v_k]p$. As X_{mean} and $[v_1,...,v_k]$ are constant, the reconstructed shape X' merely depends on the parameter vector p. In other words, p determines the difference (with respect to $[v_1,...,v_k]$) of the reconstructed shape from the mean shape X_{mean}. The range of valid values for p is derived using the training data. The combination of the range of p, X_{mean} and $[v_1,...,v_k]$ make the point distribution model (PDM).

1.2.2 Landmark Generation

In order to build a PDM that represents a sufficient proportion of the shape variation of the SNr-STN with a minimum of eigenvectors $v_1,...,v_k$, one must emphasize that it is of crucial importance that the landmarks are consistent amongst the training images. As the SNr-STN structure does not have anatomical points that could easily be identified as unique landmarks, it is non-trivial to select the required landmarks by hand. Furthermore, it is unfeasible to select several dozens of landmarks per image manually.
To overcome this problem the landmarks are generated automatically from a set of manually segmented images (training data). For the manual segmentation of the SNr-STN the open-source segmentation software ITK-SNAP [3] has been used.

1.3 Data and Preprocessing

As training images 7 MRI scans have been acquired at the Centre Hospitalier de Luxembourg using a General Electric (GE) Signa HDxt 3.0T scanner.
The used scanning protocol is a GE SWAN sequence which is an implementation of SWI [4]. The images have been acquired using 116 slices with an acquisition matrix of 512 x 512 and a square field-of-view of 240mm resulting in a voxel size of 0.4688 x 0.4688 x 1.2 mm.
Before manual segmentation, the images have been registered onto the MNI152 T1 0.5mm standard template using a non-deformable mapping method provided by the ANTs registration package [5]. An affine transformation (linear transformation and translation) is used for the mapping in order to eliminate the anisotropic voxel size and to represent all images in a common coordinate system. This common coordinate system will become helpful as a rough estimate of the SNr-STN orientation as described later.

2 Methods

The manual segmentation of the SNr-STN in the MNI152-aligned SWAN images has been performed by two neurosurgeons and two computer scientists. With that, expert knowledge of the shape of the SNr-STN is implicitly taken into account for the shape model.
As the topology of the SNr-STN on the left side and on the right side is symmetric, the right SNr-STN is matched onto the left SNr-STN using procrustes transform [6] (allowing translation, rotation and reflection). In order to reconstruct the right SNr-STN from the model, the inverse procrustes transform is applied to the landmarks that are reconstructed by the PDM.
Let $L_1,...,L_N$ be the manual segmentation of the left SNr-STN of the images $I_1,...,I_N$ and $R_1,...,R_N$ respectively be the manual segmentation of the right SNr-STN of the images $I_1,...,I_N$. $L_1,...,L_N$ and $R_1,...,R_N$ are three-dimensional binary matrices of the same size as the original images $I_1,...,I_N$, having the value 1 at index x, y, z meaning that the corresponding voxel of I with index x, y, z belongs to the SNr-STN structure and value 0 meaning that the corresponding voxel of I does not belong to the SNr-STN structure.
As only a fairly small amount of voxels, in proportion to the total number of voxels per image, belongs to the SNr-STN structure, for further processing the segmentation images are represented as a set of voxel coordinates which are represented as matrices $l_1,...,l_N$ and $r_1,...,r_N$. Each matrix has three columns, being the x, y and z coordinate of the SNr-STN voxel. In anatomical terms of location the x axis points from left to right, the y axis points from posterior to anterior and the z axis points from inferior to superior. The mapping of all right SNr-STNs to left SNr-STNs using procrustes transform leads to the combination of $l_1,r_1,...,l_N,r_N$, denoted as $s_1,s_2,...,s_{2N-1},s_{2N}$. The landmark generation for each s in $s_1,...,s_{2N}$ is performed independently.

2.1 PCA

The first step of the landmark generation is to determine the orientation of the SNr-STN structure s. In order to find the three main axes p_1, p_2 and p_3 of s a PCA is used.
Let m be the centre of gravity of s. The covariance matrix C of s is defined as $C = (s-m)^T (s-m)$. Let e_1, e_2 and e_3 be the eigenvectors of the covariance matrix C, that are sorted by their eigenvalues v_1, v_2 and v_3 in descending order. The assignment of e_1 to p_1, e_2 to p_2 and e_3 to p_3 is the first guess for the main axes of the SNr-STN segmentation s (Image 1).

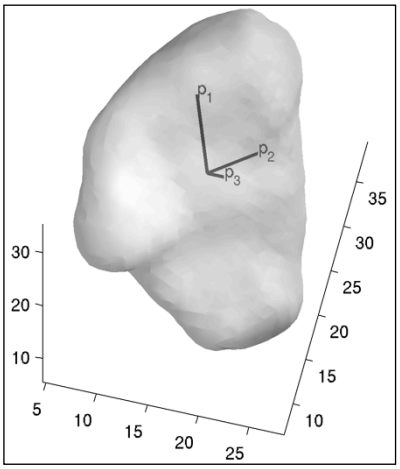

Image 1 Main axes p_1, p_2 and p_3 of the SNr-STN

2.2 Main Axes Correction

Due to the lens-like shape of the SNr-STN the eigenvectors e_1 and e_2 are not clearly separable by their eigenvalues v_1 and v_2 because they are not always considerably different. Therefore there is a chance that e_1 actually corresponds to p_2 and e_2 actually corresponds

to p_1. To overcome this problem, the assignment of the eigenvectors to the main axes is performed using simple rules. These rules are based on the premise that all images have been matched onto the MNI152 template, leading to a common coordinate system and therefore to the same SNr-STN rough-orientation. This rough-orientation is not sufficient for the determination of the main axes directly. However, in combination with the eigenvectors e_1, e_2 and e_3 this rough-orientation gives a good lead for a unique main axes assignment.
Furthermore, it is possible that the eigenvectors that are determined by the PCA point into the inverted direction. The directions of the main axes are corrected after the eigenvectors are assigned to the main axes.

2.2.1 Main Axes Assignment

The first main axis is per definition the eigenvector that is closest to parallel to the vector [0, 1, 1] (pointing anterior-superior). If the angle between e_1 and [0, 1, 1] is greater than the angle between e_2 and [0, 1, 1], and additionally $v_2 r > v_1$, the principal axis p_1 is set to e_2 and p_2 is set to e_1. The factor r determines the ratio between the eigenvalues v_1 and v_2 in order to allow a swap of p_1 with p_2. A value of 1.7 for p has been determined empirically.
As the eigenvalue v_3 of the eigenvector e_3 is always considerably smaller than the eigenvalues v_1 and v_2, the direction of e_3 is generally used as third main axis p_3.

2.2.2 Main Axes Inversion

The direction of the first main axes p_1 is inverted if the angle between p_1 and [0, 1, 1] is greater than 90^0.
As the rough direction of the third main axis p_3 is different for the left SNr-STN ([1, 0, 1], pointing right-superior) and the right SNr-STN ([-1, 0, 1], pointing left-superior), the direction p_3 for the left SNr-STN is inverted if the angle between p_3 and [1, 0, 1] is greater than 90^0 and the direction of p_3 for the right SNr-STN is inverted if the angle between p_3 and [-1, 0, 1] is greater than 90^0.
Lastly, it is checked whether the main axes form a left-handed coordinate system (LHCS) for the left SNr-STN and a right-handed coordinate system (RHCS) for the right SNr-STN respectively. If this is not the case, the direction of the second main axis p_2 is inverted. The reason for having two different coordinate systems for the left and right SNr-STN is that the right SNr-STN is transformed using a reflection so that it can be regarded as left SNr-STN and therefore the RHCS of the right SNr-STN becomes a LHCS after this reflection.

2.2.3 Manual Correction

The automatic determination of the main axes p_1, p_2 and p_3 works well with most of the data. However, if the method fails, there is the need of a manual correction. As the main axis p_3 is always determined correctly, the manual correction is enabled by the rotation of both axes p_1 and p_2 around p_3. As the main axes are the basis for the further landmark generation, it is of crucial importance that the main axes are correct before further processing. However, the manual correction is non-trivial as it requires a very thorough inspection of the morphology of the SNr-STN.

2.3 Surface Tessellation

A tessellated sphere is placed at the centre of gravity m for the landmark generation of s and then rays are cast from m through each vertex of the sphere. The intersection points of the surface of s with the rays are regarded as landmarks.

2.3.1 Sphere Generation

The sphere is created by iteratively subdividing a unit cube. Therefore the number of generated landmarks depends on the number of iterations.
In an iteration each rectangular face is subdivided into four rectangular faces (Image 2a). With the cube centred at the origin, the vertices are then normalized in order to re-establish the shape of a sphere (Image 2b-d). As the iterative subdivision leads to duplicate vertices, these duplicates are removed eventually.
In our experiments a single iteration, systematically leading to 26 unique vertices, is performed.

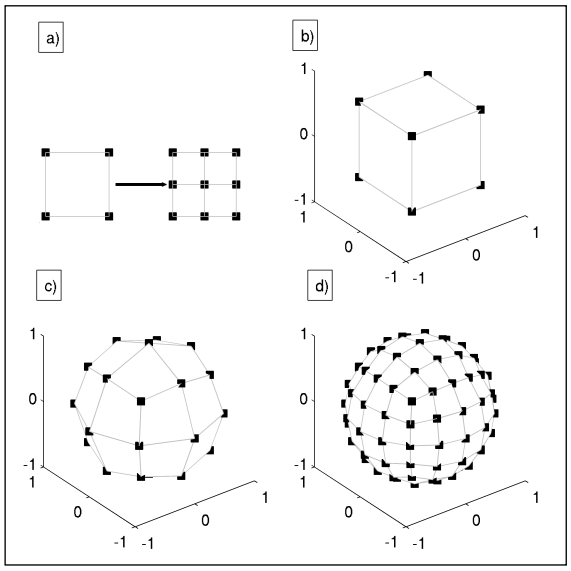

Image 2 a) Subdivision of a Rectangular Face, b) Unit Cube, c) One Iteration and d) Two Iterations

2.3.2 Sphere Transformation

The vertices of the sphere are then scaled by the eigenvalues e_1, e_2 and e_3. Subsequently the vertices are aligned by the main axes p_1, p_2 and p_3 (Image 3).

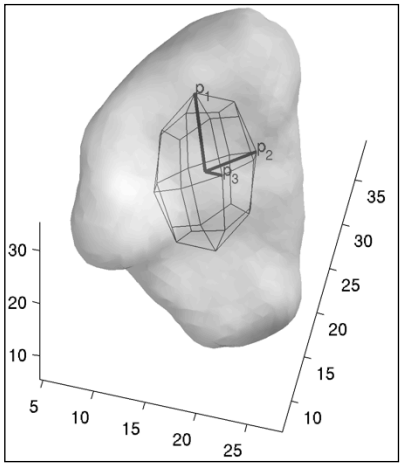

Image 3 Sphere scaled by eigenvalues and aligned by main axes

2.3.3 Landmark Generation

A ray is traced from the centre of gravity m through each of the 26 vertices. The intersection points of each ray with the hull of the SNr-STN are the landmarks (Image 4).

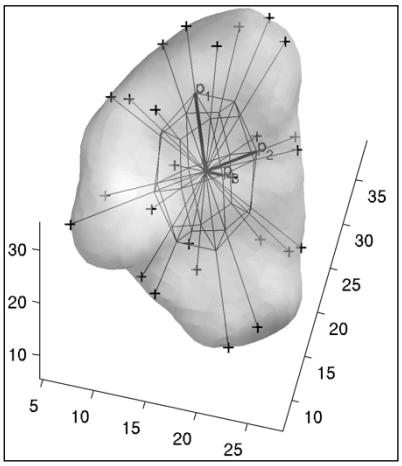

Image 4 Rays and resulting landmarks

3 Results

At the time of writing a total of 7 SNr-STN segmentations, created by two neurosurgeons and two computer scientists specialised in medical imaging, are present. 24 of the 28 segmentation images are suitable for further processing. With the right SNr-STN mapped to the left SNr-STN this leads to a total of 48 valid SNr-STN segmentations.

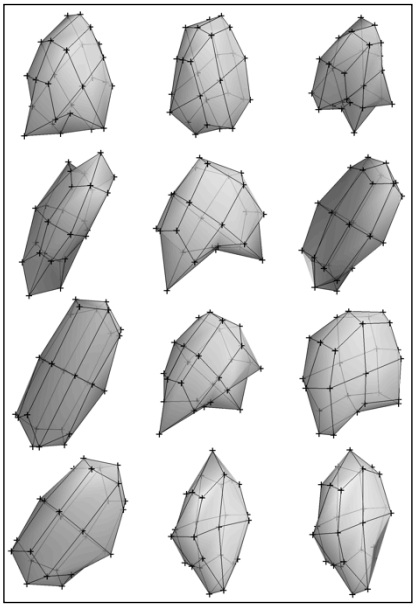

Image 5 SNr-STNs represented by landmarks

Instead of placing a total of 48□26=1248 landmarks tediously by hand, merely the 48 SNr-STNs have been segmented manually. Then, the landmark generation is performed

as described. For 36 out of the 48 segmentations (75%) the main axes are determined correctly. The remaining 12 segmentation images have been corrected manually by rotating the main axes p_1 and p_2 around p_3, which was done within a few minutes.
The evaluation of the landmarks has been done by manual inspection. Image 5 depicts the generated landmarks for a subset of the available SNr-STN segmentations.
Subsequently a PDM of the landmarks has been created. A manual adoption of the PDM parameter p within the range of $p_{mean} \pm 2\sigma$ leads to plausible SNr-STN shapes. As the PDM creation is based on the landmarks, the generation of plausible shapes is a further hint that the landmarks are of good quality.

4 Conclusion

With the semi-automatic landmark generation the first step towards an automatic STN segmentation has been reached.
However, the number of available images that have been used for the development and evaluation of the landmark generation method was rather small. Therefore the landmark generation will be evaluated with a larger patient cohort as soon as new data is available. As the landmark generation is only a part of an entire segmentation system, the full system will be implemented and analysed.

5 Acknowledgement

The project was funded by the Stiftung Rheinland-Pfalz für Innovation.

6 References

[1] Daniluk, Slawomir; Davies, Keith G.; Eollias, Samuel A.; Novak, Peter; Nazzaro, Jules M.: Assessment of the variability in the anatomical position and size of the subthalamic nucleus among patients with advanced Parkinson's disease using magnetic resonance imaging. Springer-Verlag, 2009

[2] Cootes, Tim; Taylor, Chris: Statistical Models of Appearance for Computer Vision. University of Manchester, 2001

[3] Yushkevich, Paul A.; Piven, Joseph; Hazlett, Heather Cody; Smith, Rachel Gimpel; Ho, Sean; Gee, James C.; Gerig, Guido: User-guided 3D active contour segmentation of anatomical structures: Significantly improved efficiency and reliability. NeuroImage, 31(3):1116-28, 2006

[4] Vertinsky, A.T.; Coenen, V.A.; Lang, D.J.; Kolind, S.; Honey, C.R.; Li, D.; Rauscher, A.:Localization of the Subthalamic Nucleus: Optimization with Susceptibility-Weighted Phase MR Imaging. AJNR Am J Neuroradiol, 30(9):1717-24, 2009

[5] Avants, Brian B.; Tustison, Nicholas J.; Song, Gang; Cook, Philip A.; Klein, Arno; Gee, James C.: A Reproducible Evaluation of ANTs Similarity Metric Performance in Brain Image Registration. NeuroImage, 54(3):2033-44, 2011

[6] Goodall, C.: Procrustes Methods in the Statistical Analysis of Shape. Journal of the Royal Statistical Society B, 53(2):285-339, 1991